

Short Communication

Electrochemical Behavior of Graphene/ZnO Nanoflowers Synthesized by an Efficient and Facile Two-Step Technique

Yu Zhang*, Guangjie Liu, Fanhua Yu

Department of Computer Science and Technology, Changchun Normal University, Changchun 130032, China

*E-mail: zhangy234shelly@gmail.com,

Received: 31 March 2019 / Accepted: 1 May 2019 / Published: 10 June 2019

An efficient and simple route was advanced to uniformly synthesize graphene/ZnO nanoflowers and an electrochemical impedance spectroscopy (EIS) technique was used to investigate the electrical properties. X-ray diffraction patterns indicated a broad and strong peak at 26° value, which conformed with the graphene (002) plane. A very strong Raman band appeared at 1,594 and 1,358 cm^{-1} , that corresponded to the independent G and D bands, respectively. The photoluminescence results show that the graphene/ZnO nanostructures has a lower electrons/holes recombination rate under UV light irradiation, that may be attributed to graphene sheets in graphene/ZnO nanoflowers becoming the separation mechanisms of the photogenerated electrons/holes. Cyclic voltammetry plots indicate approximately rectangular shape, showing perfect supercapacitive behavior. The charge transfer resistance in the graphene/ZnO nanoflower electrode is 175 $\text{k}\Omega$, which is considerably smaller than those of ZnO nanostructures (684 $\text{k}\Omega$) electrode, demonstrating the better conductivity in the graphene/ZnO nanoflower electrode. The graphene/ZnO nanoflowers showed excellent photocatalytic activity for the degradation of MB under the visible light which can be ascribed to the high absorption intensity of graphene/ZnO nanoflowers in visible light region.

Keywords: Graphene/ZnO nanoflowers; Electrochemical impedance spectroscopy; Cyclic voltammetry; Photoluminescence spectroscopy; Photocatalytic activity

1. INTRODUCTION

Graphene (Gr) shows many interesting optical, mechanical and electronic properties because of its two-dimensional crystal structure [1, 2]. Although, Gr being an organic compound, its charge carriers move in crystal lattice and possesses high conductivity [3, 4]. After rediscovering graphene in 2004, Gr has been strongly studied for numerous applications due to its outstanding optical, mechanical, thermal, and electrical properties [5, 6].

Recently, metal oxide semiconductors have attracted many attentions for their wide application in lithium ion batteries, transparent electronics, catalysis, hydrogen production, and water purification [7-9]. Zinc oxide (ZnO) with a high exciton binding energy and a wide band gap, is a key material possibly applicable in optoelectronic and electronic devices such as field emission, solar cells, sensors and displays [10-12].

Due to the wonderful individual properties of ZnO and graphene, the combination of both these nanostructures can enhance performances. A number of studies have been done to generate graphene/ZnO hybrids. The photoluminescence properties of vertically growth ZnO nanostructures on graphene films was reported by Kim et al. using non-catalytic vapor-phase epitaxy [13]. Wu et al. applied a hydrothermal route to synthesize sandwich-like hybrid ZnO-graphene materials using zinc acetylacetonate and graphene oxide (GO) precursors [14]. Jabeen et al. prepared ZnO-graphene nanocomposites through the UV-assisted photocatalytic synthesis of reduced GO in ZnO suspensions [15]. Ali et al. generated ZnO-graphene hybrids layers using ultrasonic spray pyrolysis [16]. In addition, Sreejesh et al. synthesized ZnO-graphene hybrids [24] through the microwave-assisted technique by reducing Zn^{2+} ions in the solution with GO [17].

However, most of the experimental methods reported are still limited by the laboratory scale because of some unsolved issues, such as special conditions, complex apparatus or tedious procedures, high cost and low yield. In this research, graphene/ZnO nanoflowers were synthesized by an efficient and facile two-step technique. Electrochemical impedance spectroscopy (EIS) was performed as a suitable technique to consider the electrical properties of graphene/ZnO nanoflower materials. Furthermore, a study on photocatalytic activities of graphene/ZnO nanoflowers were done using visible light as a source of radiation and methylene blue (MB) as the test contaminant.

2. MATERIALS AND METHODS

The synthesis of the graphene/ZnO nanoflowers were done in two-step. First, GO was produced by oxidizing purified natural graphite using the modified Hummer's technique [18]. 0.05 gL^{-1} GO aqueous suspension was spin-coated on fluorine-doped tin oxide (FTO) to achieve few-layer GO thin films. Then, GO film was reduced to graphene layer on FTO/glass in vapor-phase hydrazine at $70\text{ }^{\circ}\text{C}$ for 8 hours. The thickness of the layer was controlled by doing the spin-coating procedure several times. In the second step, an aqueous solution method was used to grow ZnO nanoflowers on FTO/glass substrate. An equimolar mixture (0.1M) of hexamethylenetetramine (HMT) and zinc nitrate hexahydrate were dissolved in distilled water. The aqueous solution mixture was stirred for twenty minutes to make a homogeneous mixture. The 25 mM aqueous solution was put into a cell. The samples were transferred to the cell and maintained at $95\text{ }^{\circ}\text{C}$ for 3 h and then allowed to cool to room temperature. After that, the samples were taken out, washed and dried.

The samples were characterized by field emission scanning electron microscopy (FE-SEM, FEI Sirion 200) analysis. X-ray diffraction (XRD, Rigaku D/max 2500 PC diffractometer) was done using CuK α radiation in the 2θ range of $10\text{--}80^{\circ}$. Photoluminescence (PL) measurements of the graphene/ZnO nanostructures were carried out at $25\text{ }^{\circ}\text{C}$ and a 300 nm excitation wavelength. Raman

spectra were recorded on Lab RAM HR 800 microspectrometer (Jobin-Yvon) using a 514.5 nm argon laser. The UV-vis spectra of the graphene/ZnO nanoflowers were carried out by a UV-vis spectrophotometer (UV-1800, Shimadzu, Kyoto, Japan). The electrochemical analysis was done in a typical three-electrode cell using an Ag/AgCl electrode reference electrode, a Pt plate counter electrode and an FTO modified graphene/ZnO working electrode. The electrolyte was 0.2 M Na₂SO₄ aqueous solution without additive (pH = 6.8). Cyclic voltammetry (CV) was carried out in potential ranges of 0.8 V to -0.6 V and the scanning rate of 20 mV s⁻¹. The photocatalytic performance of K-doped ZnO nanopapers were assessed by the degradation of MB dye under UV and sunlight irradiation. The study of photocatalytic activities was assessed by the decomposition of methylene blue (MB) under visible light irradiation. 10 mgL⁻¹ MB aqueous solution was transferred to a container. Before the irradiation, the solution was magnetically stirred in the dark for about 30 min.

3. RESULTS AND DISCUSSION

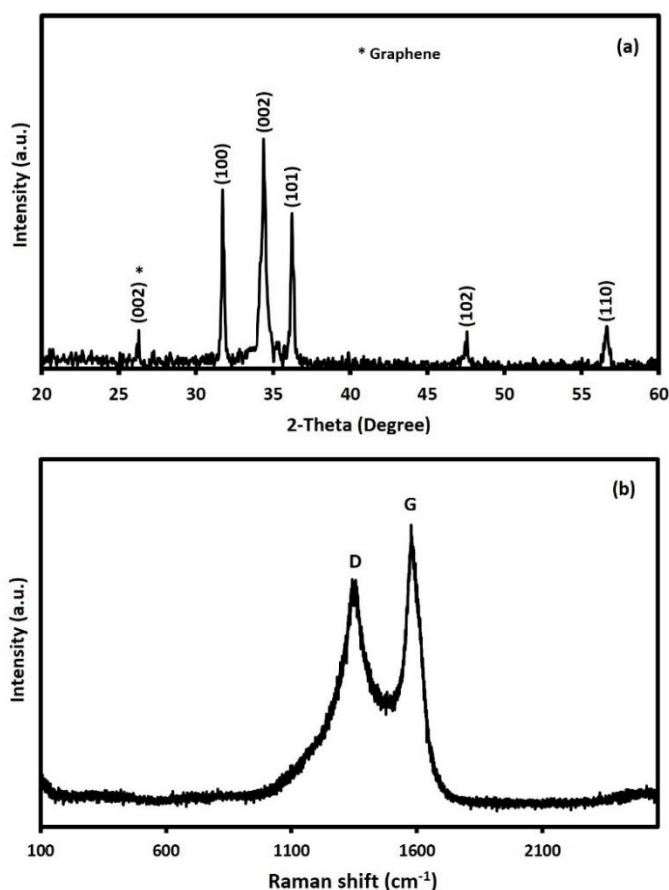


Figure 1. (a) the typical XRD patterns and (b) the Raman spectra of the as-synthesized graphene/ZnO nanoflowers grown on FTO/glass at growth temperature of 95 °C and growth time of 3 h

Figure 1a indicates the XRD patterns of the as-synthesized flower-like graphene/ZnO nanostructures. It is shown that the XRD pattern contains five diffraction peaks at 31.7°, 34.4°, 36.2°, 47.5°, and 56.6°.

47.5°, and 56.5, matching to the (100), (002), (101), (102), and (110) planes of the ZnO hexagonal phase with wurtzite structure (Reference pattern: 01-080-0075), respectively. Furthermore, a broad and strong peak was found at a 2θ value nearly 26° , which conformed with the graphene (002) plane. There are no other peaks from GO indicating GO is absolutely reduced to a graphene layer.

The graphene Raman spectra are generally considered by two prominent peaks; a weak D-band peak centered at around 1350 cm^{-1} and a strong G-band peak centered at around 1590 cm^{-1} [19]. These bands are in agreement with the E_{2g} optical mode Raman-active phonon and the breathing A_{1g} mode at around k-point which are allocated to local disorder and defects at the edges of graphite and graphene platelets [20]. Figure 1b indicates the Raman spectra of as-synthesized graphene/ZnO nanoflower structures. A very strong Raman band appeared at $1,594$ and $1,358\text{ cm}^{-1}$, that corresponded to the independent G and D bands, respectively. The G band has valuable information about the in-plane vibration mode of sp² hybridized carbon atoms in two dimensional hexagonal lattice and the D-band is a general feature for sp³ disorder or defects in carbon.

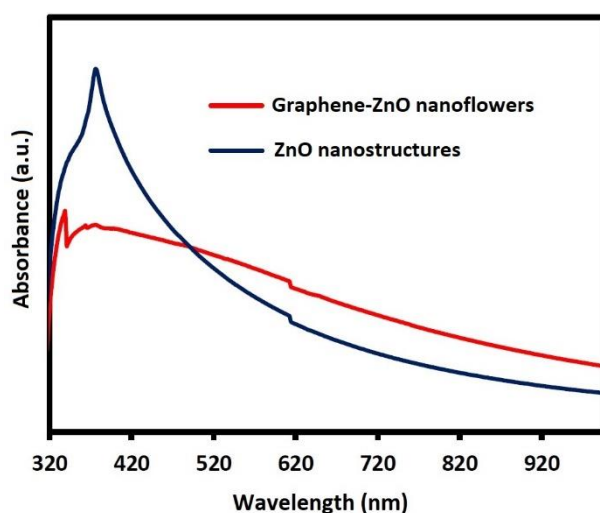


Figure 2. UV–Vis absorbance spectra of blank ZnO nanostructures and graphene/ZnO nanoflowers grown on FTO/glass at growth temperature of 95°C and growth time of 3 h

The UV-vis absorbance spectra are utilised to consider the Optical properties in the visible and UV of the specimens. As shown in Figure 2, the reduced GO has a considerable effect on the absorption of the graphene/ZnO nanoflowers which lead to the enhancement of the visible light absorption in ranges of 450 to 950 nm. However, the optical-absorption edge of graphene/ZnO nanostructures is comparable to that of ZnO nanostructures, indicating that both bare ZnO nanostructures and graphene/ZnO nanostructures may be band-gap-photoexcited via UV light irradiation.

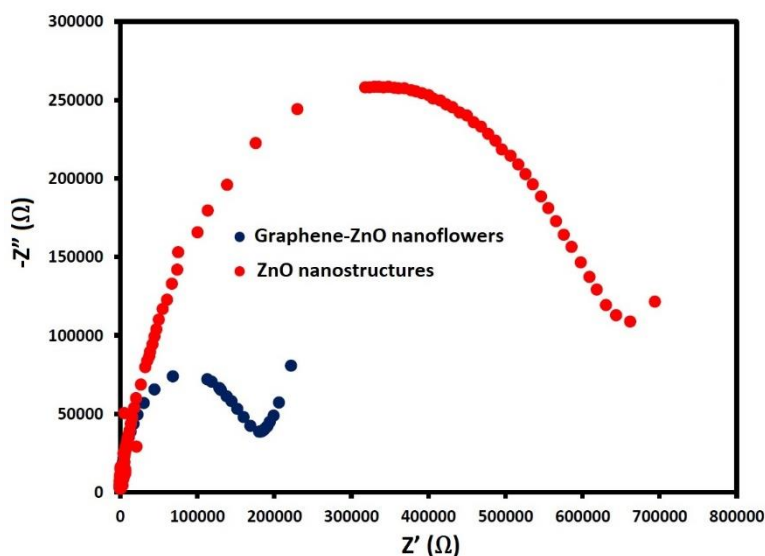


Figure 3. EIS Nyquist plots of ZnO nanostructures and graphene/ZnO nanoflowers in 0.2 M Na₂SO₄ aqueous solution as electrolyte without additive (pH = 6.8)

To further study the advantage of graphene/ZnO nanoflowers over ZnO nanostructures in enhancement of the charge carriers transfer, CV and EIS Nyquist plots have been performed to describe the charge-carrier migration. EIS was shown to realize the conductivity, mechanistic investigation of interfacial processes, and electron transport in the electrode-electrolyte interface. Figure 3 indicates the Nyquist diagrams for the graphene/ZnO nanoflowers and ZnO nanostructure electrodes. These plots show a straight line at the lower frequency region and a semicircle at the higher frequency region. The straight line at the low-frequency is named the Warburg resistance, that is due to the frequency-dependent of ion diffusion from the electrolyte to the surface area of electrodes [21, 22]. In the high frequency range, the arc corresponded to the limiting process of the charge transfer and was attributed to a charge transfer resistance (R_{CT}) in parallel to a double-layer capacitance at the interface between the electrolyte solution and electrode. The R_{CT} may be directly determined from the Nyquist diagrams as the diameter of semicircular arc. The R_{CT} in the graphene/ZnO nanoflower electrode is 175 k Ω , which is considerably smaller than those of ZnO nanostructures (684 k Ω) electrode, demonstrating the better conductivity in the graphene/ZnO nanoflower electrode. It shows the growth of ZnO nanorods onto the graphene layers, resulting in an enhancement of charge transfer act in the electrode. Furthermore, the graphene/ZnO nanoflowers show depressed semicircles in high frequencies compared to the ZnO nanostructures, which proposes a reduction in the resistance of interface layer. Specifically, the integration of ZnO nanoflowers with graphene enhances the charge carrier transfer.

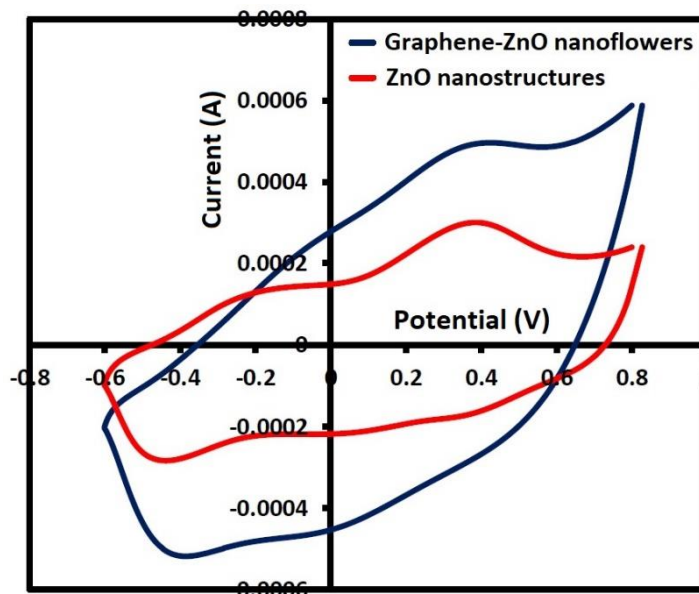


Figure 4. Cyclic voltammograms of ZnO nanostructures and graphene/ZnO nanoflowers in potential ranges of 0.8 V to -0.6 V and the scanning rate of 20 mV s^{-1} .

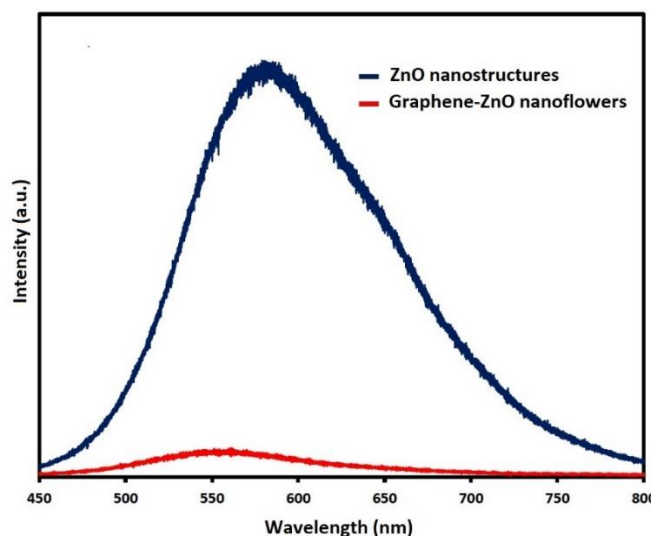


Figure 5. Room temperature photoluminescence spectra of ZnO nanostructures and graphene/ZnO nanoflowers grown on FTO/glass at growth temperature of $95 \text{ }^\circ\text{C}$ and growth time of 3 h

In order to indicate the benefit of the graphene/ZnO nanoflowers, Figure 4 shows a comparison of the cyclic voltammetry plots of ZnO nanostructures and graphene/ZnO nanoflowers. It clearly observed cathodic and anodic and peaks in the CV for each specimen. Given that the preparation of the electrolyte and electrodes are the same for the measurement of CV curve; the current density on the surface of electrodes is associated to the rate of electron transfer in the electrode materials. As shown in the figure 4, these plots indicate approximately rectangular shape, showing perfect supercapacitive

behavior. The graphene/ZnO flower-like nanostructure electrode exhibited a higher integrated area than the ZnO nanostructures, which indicates the excellent electrochemical performance in the graphene/ZnO nanoflowers electrode.

Figure 5 shows PL spectrum of ZnO nanostructures and graphene/ZnO nanoflowers in a broad visible light band at 450–800 nm and a peak at around 580 nm, which is ascribed to the oxygen-vacancy defects in the lattice of ZnO. For the graphene/ZnO nanoflowers, the noticeably decreased emission intensity indicates an efficient interfacial charge-transfer process, indicating that a further pathway for vanishing the charge carriers, due to the interactions between the graphene sheets and excited ZnO nanoflowers. This shows that the graphene/ZnO nanostructures has a lower electrons/holes recombination rate under UV light irradiation, that is generally because of the excited electrons from the valence to the conduction bands of ZnO nanoflowers and later are transferred to graphene layers, avoiding a direct electrons/holes recombination. This may be attributed to graphene sheets in the graphene/ZnO nanoflowers are becoming the separation mechanisms of the electrons/holes and due to this property, these layers are investigated to be an alternative electron acceptor material to efficiently hinder the recombination of electron/hole pairs because of its two-dimensional π -conjugation structure [23, 24].

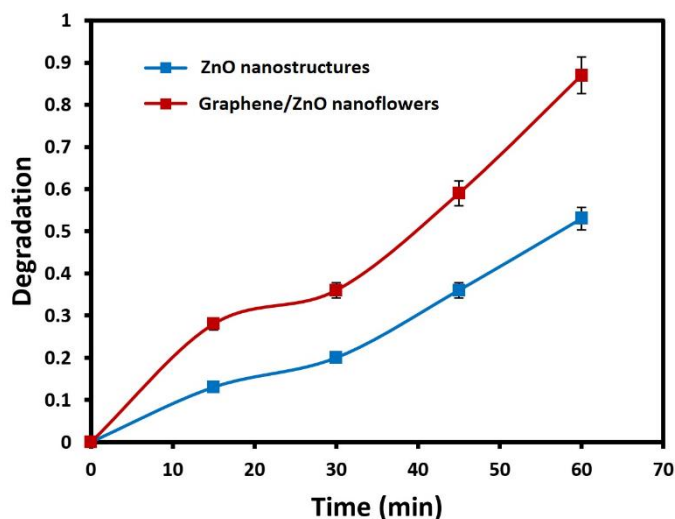


Figure 6. The photocatalytic activity of ZnO and graphene/ZnO nanoflowers under visible light (20 ppm MB dye concentration and 100 mg catalytic load at pH 7)

The photocatalytic activity of as-synthesized samples under visible light is shown in Figure 6. As shown, the graphene/ZnO nanoflowers indicate superior photocatalytic efficiency compared to ZnO nanostructures, it can be related to the high absorption intensity of graphene/ZnO nanoflowers in visible light region which can improve the separation of photogenerated electron/hole pairs and inhibit the excited electron-hole recombination to enhance the photocatalytic properties.

The literature survey indicates that the most recent studies of photodegradation have been conducted using Photocatalytic degradation method [25-27]. Comparison between some previously published techniques and the present study are summarized in table 1. The results show that

graphene/ZnO nanoflowers photocatalysis can be considered as one of the effective water treatment methods in the future.

Table 1. Photodegradation comparison under visible light irradiation

Samples	Growth technique	Degradation efficiency	Degradation time	Ref.
Graphene–ZnO nanoparticles	Aqueous solution technique	70%	3 h	[25]
ZnO nanowires	Hydrothermal method	74.7%	2 h	[26]
Graphene oxide/ZnO nanorod films	Hydrothermal method	87%	7.5 h	[27]
Graphene/ZnO nanoflowers	Aqueous solution technique	~ 90%	1 h	This work

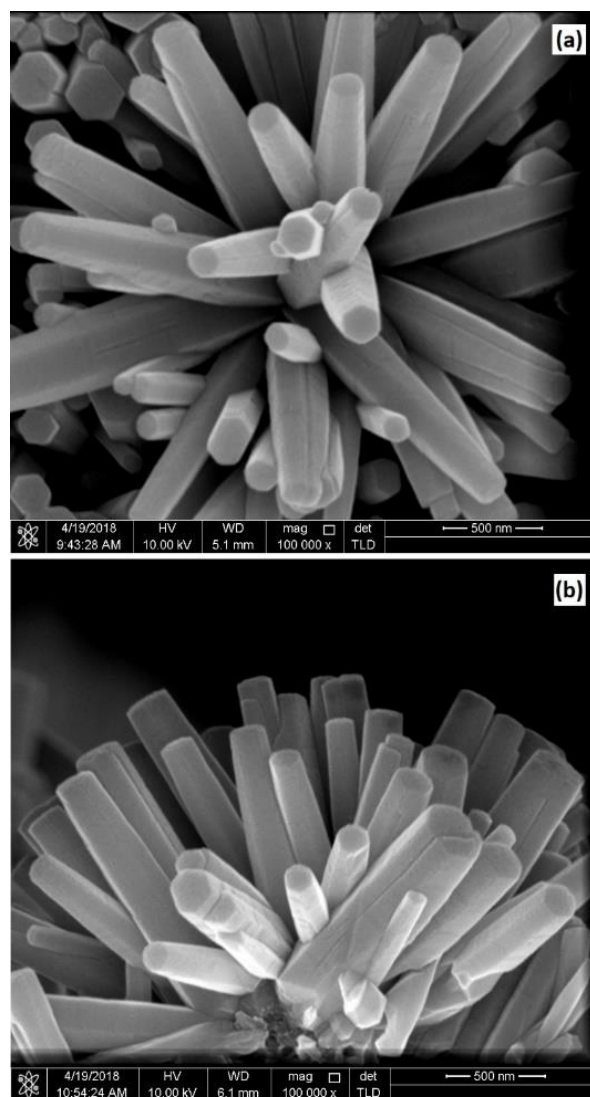


Figure 7. (a) Top view and (b) Cross section FESEM images of graphene/ZnO nanoflowers grown on FTO/glass at growth temperature of 95 °C and growth time of 3 h

The FESEM images of The flower-like graphene/ZnO nanorods are shown in figure 7. The hexagonal wurtzite structure of the ZnO nanostructures help anisotropic growth along a vertical direction [0001] which results in a rod-like structure.

4. CONCLUSION

In this research, graphene/ZnO nanoflowers were synthesized by an efficient and facile two-step technique. Electrochemical impedance spectroscopy (EIS) was performed as a suitable technique to consider the electrical properties of graphene/ZnO nanoflower materials. The PL spectrum of ZnO nanostructures and graphene/ZnO nanoflowers indicated a broad visible light band at 450–800 nm and a peak at around 580 nm, which was ascribed to the oxygen-vacancy defects in the lattice of ZnO. The R_{CT} in the graphene/ZnO nanoflower electrode was 175 k Ω , which was considerably smaller than those of ZnO nanostructures (684 k Ω) electrode, demonstrating the better conductivity in the graphene/ZnO nanoflower electrodes. The graphene/ZnO flower-like nanostructure electrode exhibited a higher integrated area than the ZnO nanostructures, which indicated an excellent electrochemical performance in the graphene/ZnO nanoflowers electrode. Furthermore, the graphene/ZnO nanoflowers had shown an excellent photocatalytic activity for the degradation of MB under the visible light which can be ascribed to the high absorption intensity of graphene/ZnO nanoflowers in visible light region

ACKNOWLEDGEMENT

This work was supported by National Natural Science Foundation of China (Grant No. 61604019, Project supported by science and technology development project of Jilin Province, China (Grant No. 20160520098JH) and supported by the talent introduction scientific research project of Changchun Normal University, China (Grant No.RC2016009) .

References

1. W. Choi, N. Choudhary, G.H. Han, J. Park, D. Akinwande and Y.H. Lee, *Materials Today*, 20 (2017)
2. K.F. Mak and J. Shan, *Nat. Photonics*, 10 (2016) 216.
3. A.C. Ferrari, F. Bonaccorso, V. Fal'Ko, K.S. Novoselov, S. Roche, P. Bøggild, S. Borini, F.H. Koppens, V. Palermo and N. Pugno, *Nanoscale*, 7 (2015) 4598.
4. S.H. Dave, C. Gong, A.W. Robertson, J.H. Warner and J.C. Grossman, *ACS nano*, 10 (2016) 7515.
5. S. Ramirez, K. Chan, R. Hernandez, E. Recinos, E. Hernandez, R. Salgado, A. Khitun, J. Garay and A. Balandin, *Mater. Des.*, 118 (2017) 75.
6. S. Colonna, O. Monticelli, J. Gomez, C. Novara, G. Saracco and A. Fina, *Polymer*, 102 (2016) 292.
7. M. Husairi, J. Rouhi, K. Alvin, Z. Atikah, M. Rusop and S. Abdullah, *Semicond. Sci. Technol.*, 29 (2014) 075015.
8. K. Eswar, J. Rouhi, H. Husairi, M. Rusop and S. Abdullah, *Adv. Mater. Sci. Eng.*, 2014 (2014) 1.
9. J. Socratous, K.K. Banger, Y. Vaynzof, A. Sadhanala, A.D. Brown, A. Sepe, U. Steiner and H. Siringhaus, *Adv. Funct. Mater.*, 25 (2015) 1873.

10. J. Rouhi, S. Mahmud, S. Hutagalung and N. Naderi, *Electron. Lett.*, 48 (2012) 712.
11. R. Dalvand, S. Mahmud, J. Rouhi and C.R. Ooi, *Mater. Lett.*, 146 (2015) 65.
12. J. Rouhi, C.R. Ooi, S. Mahmud and M.R. Mahmood, *Mater. Lett.*, 147 (2015) 34.
13. Y.-J. Kim, J.-H. Lee and G.-C. Yi, *Appl. Phys. Lett.*, 95 (2009) 213101.
14. J. Wu, X. Shen, L. Jiang, K. Wang and K. Chen, *Appl. Surf. Sci.*, 256 (2010) 2826.
15. M. Jabeen, M. Ishaq, W. Song, L. Xu, I. Maqsood and Q. Deng, *ECS J. Solid State Sci. Technol.*, 6 (2017) M36.
16. A.A. Ali and A.M. Hashim, *Nanoscale Res. Lett.*, 10 (2015) 452.
17. M. Sreejesh, S. Dhanush, F. Rossignol and H. Nagaraja, *Ceram. Int.*, 43 (2017) 4895.
18. J. Chen, Y. Li, L. Huang, C. Li and G. Shi, *Carbon*, 81 (2015) 826.
19. Z. Ling, Z. Wang, M. Zhang, C. Yu, G. Wang, Y. Dong, S. Liu, Y. Wang and J. Qiu, *Adv. Funct. Mater.*, 26 (2016) 111.
20. R. Beams, L.G. Cançado and L. Novotny, *J. Phys. Condens. Matter*, 27 (2015) 083002.
21. E.J. Lee, L. Lee, M.A. Abbas and J.H. Bang, *Phys. Chem. Chem. Phys.*, 19 (2017) 21140.
22. K. Castro, S. Oliveira, R. Curti, J. Araujo, L. Sassi, C. Almeida, E. Ferreira, B. Archanjo, M. Cabral and A. Kuznetsov, *Int. J. Electrochem. Sci.*, 13 (2018) 71.
23. A.K. Geim, *science*, 324 (2009) 1530.
24. Q. Xiang, J. Yu and M. Jaroniec, *J. Phys. Chem. C*, 115 (2011) 7355.
25. T. Kavitha, A.I. Gopalan, K.-P. Lee and S.-Y. Park, *Carbon*, 50 (2012) 2994.
26. Q. Zhou, J. Wen, P. Zhao and W. Anderson, *Nanomaterials*, 7 (2017) 9.
27. E. Rokhsat and O. Akhavan, *Appl. Surf. Sci.*, 371 (2016) 590.